Excerpt from the Proceedings of the 2011 COMSOL Conference in Boston

MEMS-Based Microdroplet Generation with Integrated Sensing

William S. Rone and Pinhas Ben-Tzvi*
Robotics and Mechatronics Laboratory, School of Engineering and Applied Science
The George Washington University
*Corresponding author: 801 22nd St NW, Washington, DC 20052, bentzvi@gwu.edu

Abstract: This paper presents the development of a two-dimensional axisymmetric finite element model used to simulate a microdroplet generator capable of internally sensing the volumes of droplets it dispenses. This integrated sensing is enabled by storing compressible gas adjacent to the dispenser's droplet liquid reservoir. During and after actuation, the volume/pressure of the compressible gas will change. It is hypothesized that this pressure change profile could be utilized to measure the ejected droplet's volume. To numerically validate this hypothesis, COMSOL Multiphysics v4.0a's Laminar Multi-Phase Flow, Level-Set physics were utilized. Fluid-structure interaction was modeled as a variable pressure boundary condition, and the COMSOL Materials Library was utilized for the liquid (water) and gas (air). The results show a linear coupling between the maximum pressure change in the gas reservoir and ejected droplet volume. However, this relation was only valid above an actuation magnitude threshold to ensure droplet ejection.

Keywords: MEMS, microfluidics, microdroplet generation, compressible flow, level-set method

1. Introduction

Microdroplet generation has developed into a critical field in microfluidics to enable the scaling of macro-scale techniques onto the microscale. From biological and chemical analysis/synthesis [1,2] to medicine [3,4] to manufacturing [5,6], technologies able to reliably discretize liquids into microdroplets are necessary to advance both scientific inquiry and technological development. For a more detailed analysis of the field, see [7].

However, there has been a lack of focus on real-time sensing to quantify ejected droplet volumes during droplet generation. Furthermore, of technologies currently available to measure dispensed droplet volumes, the focus has been on external instrumentation, such as cameras [8] or balances [9]. Limited research has been performed into integrating sensing into the system to improve its operation [10,11].

This paper describes the analysis of a novel design concept [12,13] to enable integrated sensing of droplet volumes during generation. The design utilizes a compressible gas stored adjacent to an incompressible liquid in the generator's fluid reservoir to relate the volume of liquid ejected to the pressure of the compressible gas. By sensing the pressure of the gas, the volume of the droplet can be indirectly measured.

In this paper, Section 2 further describes the design concept and its adaptation into a finite element (FE) model. Section 3 describes the solution process and the results obtained from the analyses. Section 4 summarizes the work and describes planned future work.

2. Design Concept and Modeling

Figure 1 illustrates the microdroplet generator under consideration. Liquid is stored in a capillary chamber, with a gas reservoir present at one end and a nozzle at the other. The cap at the end of the capillary is flexible and is bonded to a sensor capable of measuring the pressure in the chamber through the deflection of the cap. A piezoelectric actuator is bonded to the outer surface of the capillary and is polarized to radially expand and contract.

In order to generate a droplet, a potential difference is applied over the piezo-actuator, contracting then releasing it. During this motion, the gas reservoir will vary in pressure, which is measured by the sensor integrated into the cap. After droplet ejection, the pressure in the gas will stabilize but will experience a change in magnitude from its initial state, due to the slight depletion of liquid from the chamber. This magnitude of pressure change is related to the volume dispensed, allowing for measurements of this pressure change to "close-the-loop" between desired droplet volumes and actual droplet volumes.

COMSOL Multiphysics was chosen for the numerical studies because of its flexibility in

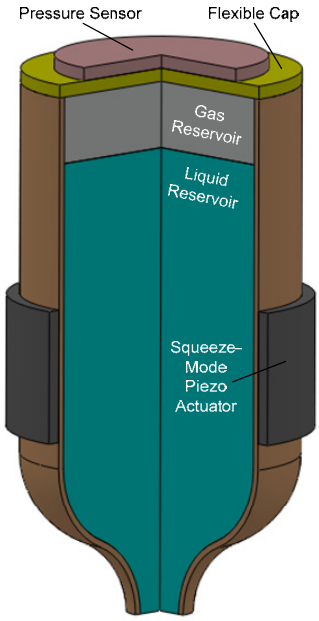

Figure 1. Microdroplet generator design concept

generating and solving the model using a variety of numerical techniques and solvers (e.g. allowing use of either level-set or phase field for multi-phase fluid tracking). Furthermore, use of COMSOL will allow for more advanced simulations incorporating fluid-structure interaction and piezoelectric models to be seamlessly integrated with our current work in the future.

From the design concept in Figure 1, a 2D axisymmetric geometric model was developed, as shown in Figure 2(a). This 2D assumption was made in order to simplify the computation because the actuator does not cause the liquid in the capillary to circulate around the axis of symmetry. The flow focusing region was modeled with a straight line instead of a curve to reduce mesh complexity. Dimensions are based on another droplet generator studied in the literature [14].

The COMSOL Material Library was used to model the liquid and gas phases within the simulation. Water was chosen as the liquid phase, due to a large proportion of water-based solutions dispensed in laboratory settings. Air was used in both the compressible gas reservoir and downstream of the nozzle. An ambient temperature of 25 °C was prescribed, and the pressure of each fluid was coupled to the

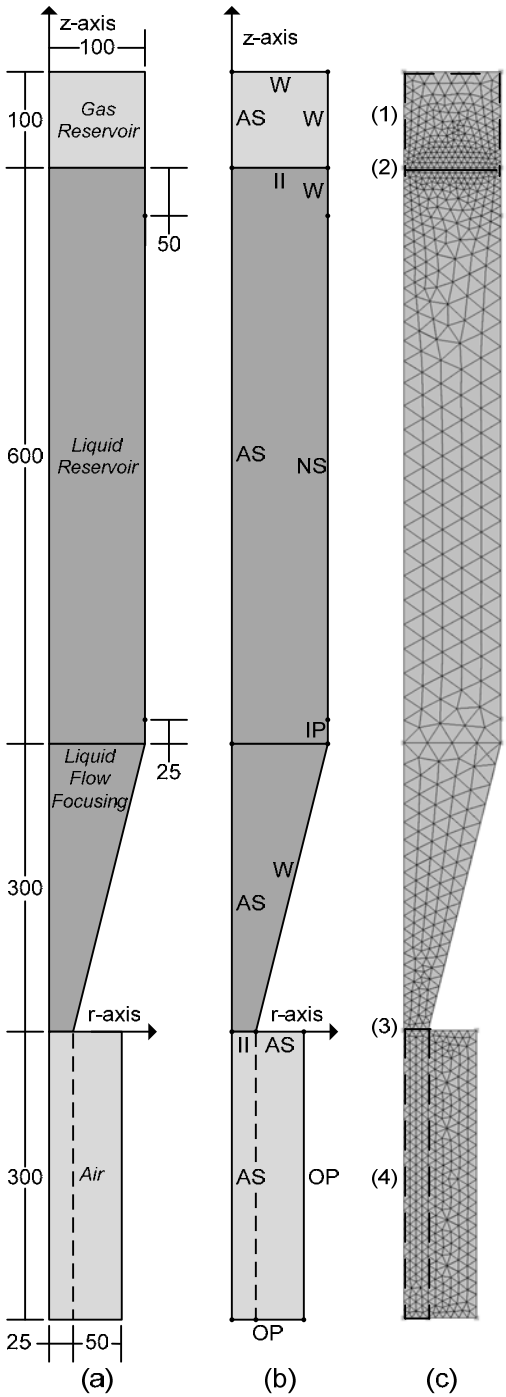

Figure 2. 2D axisymmetric model: (a) geometry, (b) boundaries, (c) mesh

pressure field variable. Relevant properties modeled for each fluid include density and viscosity. For the liquid, both remain constant (each is only coupled to the constant

temperature). For the gas, the pressure variations affect density (viscosity remains constant).

In order to accurately model the problem, three variables must be solved for at each node: a scalar pressure (p), a two-component velocity vector ($\boldsymbol{v} = [v_r \quad v_z]^T$) and a scalar level-set value (ϕ). The pressure and velocity govern the motion and state of the fluid, while the level-set governs the two-phase fluid interaction.

Equations 1-3 are utilized to solve for these variables. To simplify analysis, these equations are considered in Cartesian form, though COMSOL will automatically convert them to cylindrical coordinates and set the azimuthal terms (θ, v_θ, etc.) to zero.

$$\frac{\partial \rho}{\partial t} + \rho \nabla \cdot \boldsymbol{u} = 0 \tag{1}$$

$$\rho \frac{\partial \boldsymbol{u}}{\partial t} + \rho(\boldsymbol{u} \cdot \nabla)\boldsymbol{u} = \nabla \cdot \left[-p\boldsymbol{I} + \mu(\nabla \boldsymbol{u} + (\nabla \boldsymbol{u})^{\mathrm{T}}) - \frac{2}{3}\mu(\nabla \cdot \boldsymbol{u})\boldsymbol{I}\right] + \rho \boldsymbol{g} + \boldsymbol{F} \tag{2}$$

$$\frac{\partial \phi}{\partial t} + \nabla \cdot (\boldsymbol{u}\phi) = \gamma \nabla \cdot \left(\varepsilon_{ls} \nabla \phi - \phi(1-\phi)\frac{\nabla \phi}{|\nabla \phi|}\right) \tag{3}$$

Equation 1 represents the conservation of mass, where ρ is density and $\boldsymbol{u} = [u \quad v \quad w]^T$ is the fluid velocity vector. The left-hand term represents the total derivative of the density of the fluid, and this derivative will be zero everywhere.

Equation 2 is the conservation of momentum, where μ is the absolute viscosity, $\boldsymbol{g}$ is the gravity vector and $\boldsymbol{F}$ is the external force vector. The left-hand terms account for total derivative of momentum and equates to the sum of the divergence of the internal stress, gravitational effects and external force.

Equation 3 controls the evolution of the fluid distribution, manifested in the level-set variable. The left-hand terms represent the total derivative of the level-set variable. The right hand terms are utilized for numerical stabilization, with γ controlling the damping of oscillations/numerical instabilities and ε_{ls} controlling the thickness of fluid interfaces.

For the model's "Fluid Properties," a constant temperature of 293.15 K was utilized to mimic ambient temperature, and the pressure was coupled to the system's gage pressure variable after conversion to absolute pressure. The surface tension utilizes the built-in water-air interface properties. The level-set reinitialization parameter was set to 5 m/s (the maximum expected fluid velocity) and the interface thickness was set to half of the maximum mesh length in each subdomain.

"Initial Value" modules were used to distinguish the two fluids as illustrated by the shading in Figure 2(a). The pressure throughout the system was initialized to atmospheric, and the velocity everywhere was initialized to zero. A "Gravity" module was added to incorporate a gravitational force in the $-z$ direction.

Figure 2(b) highlights the boundaries of the geometric model of the system. Relevant boundaries are labeled, and the labels are summarized in Table 1 and described in further detail below.

Table 1. Summary of boundary conditions

AS	Axial Symmetry	II	Initial Interface
IP	Inlet – Pressure, No Viscous Stress	OP	Outlet – Pressure, No Viscous Stress
NS	Wall – No Slip	W	Wall - Wetted

Axial Symmetry (AS) ensures that singularities are avoided at the axis of symmetry of the 2D axisymmetric model. Radial velocities are constrained to zero ($v_r = 0$) and stresses vanish in the z-direction.

Inlet–Pressure, No Viscous Stress (IP) is used to mimic the fluid-structure interaction indirectly by prescribing the pressure within the liquid reservoir. This pressurized reservoir forms a droplet at the outlet and acts upon the gas reservoir. Three Heaviside functions are utilized to create the desired pressure profile, as shown in Equation 4, and a pressure magnitude is multiplied by this function for the prescribed time-varying pressure. This actuation pressure magnitude was used as the control variable in the simulation, with its variations determining whether or not a droplet ejects, and if it does, what its size is. The function shown mimics the contracting and relaxing action of the piezo by initially pressurizing the liquid, then rapidly changing to a negative pressure, then relaxing back to atmospheric.

$$\begin{aligned}&\text{flc1hs}\left(t\left[\frac{1}{s}\right]-1.5\text{e}-6,1.5\text{e}-6\right)\\&-2*\text{flc1hs}\left(t\left[\frac{1}{s}\right]-4\text{e}-6,1\text{e}-6\right)\\&+\text{flc1hs}\left(t\left[\frac{1}{s}\right]-6.5\text{e}-6,1.5\text{e}-6\right)\end{aligned}\quad(4)$$

This region of the boundary was made relatively small compared to the length of the piezo-actuator illustrated in Figure 1. This is because once the increase and decrease in pressure occur, this boundary will continue to prescribe zero pressure along its length. However, after actuation in the actual system, the pressure will be allowed to equilibrate naturally. If this inlet is too large, the forced pressure will prevent equilibration within the system, affecting droplet ejection and the gas reservoir pressure. Furthermore, this inlet was made to be composed solely of liquid ($\phi = 0$) and to impose no viscous stress ($[\mu(\nabla \boldsymbol{u} + (\nabla \boldsymbol{u})^T)]\boldsymbol{n} = \boldsymbol{0}$), where $\boldsymbol{n}$ is the vector normal to the inlet surface.

Outlet – Pressure, No Viscous Stress (OP) is used along the outer edges of the gas region downstream of the nozzle. As a droplet forms at the nozzle, it will push the gas previously occupying that space away from the nozzle. This outlet prevents any boundary effects at the edges of the mesh in this region by allowing the gas to flow out of the system. The pressure at these outlets is prescribed to be atmospheric ($p = 0$) and there is no viscous stress ($[\mu(\nabla u + (\nabla u)^T)]\boldsymbol{n} = 0$).

Wall – Wetted (W) is used surrounding the outer edges of the gas reservoir to allow the interface to move along the wall. If a no-slip condition were used, the interface would remain at its initial position along the capillary. This condition prescribes that fluid velocities normal to the wall vanish ($\boldsymbol{n} \cdot \boldsymbol{u} = 0$) and that the frictional force on the fluid be prescribed as $F_{fr} = -\frac{\mu}{\beta}\boldsymbol{u}$, where β is the slip length. In this simulation, the slip length is coupled to the mesh length at each element.

Wall – No Slip (NS) is used at all other locations along the outside of the model. This is a standard assumption for any wall abutting a single-phase flow. The boundary constrains the fluid velocity to be zero ($\boldsymbol{u} = \boldsymbol{0}$).

Initial Interface (II) is used at internal boundaries of the model where the two fluid phases are initially separated. This prescribes the level-set function to be initially set to $\phi = 0.5$. This boundary is critical in the level-set variable initialization (described in Section 3) to enable the level-set variable to be smoothed over these discontinuous boundaries.

All other interfaces not specified utilize a continuity boundary condition to ensure continuous variable fields across the subdomains.

Based on the system geometry and the subdomain/boundary requirements, a triangular unstructured mesh was generated on which to solve the model, as shown in Figure 2(c). A series of controls were placed on the mesh to ensure sufficient accuracy in critical locations in the simulation while minimizing computational complexity. In domain (1), the maximum element growth rate was constrained to be 1.08, while in domain (4) the growth rate was set to 1.05 and the maximum element size was set to 1e-5. At boundary (2), the maximum element size was limited to 6.5e-6. At boundary (3), the predefined “Extra Fine” control was used to begin the mesh, but an additional control of 8.5e-6 maximum element size was also imposed. These were determined through a series of simulations running identical models, but with variations in mesh parameters, testing for repeatability, convergence and solution time.

An unstructured triangular mesh was chosen over both structured and unstructured quadrilateral meshes because of its improved stability and efficiency. Structured meshes require large numbers of elements, propagating the fine mesh requirements in critical areas throughout the entire model. Unstructured meshes allow for a more targeted refinement. Unstructured quadrilaterals were found to be less stable than triangles – models that would readily solve with a triangular mesh would diverge on the quad mesh.

3. Simulation and Results

After generating the finite element model of the design concept, including geometry, subdomain properties, boundary properties and mesh, a sequence of steps to solve the model were formulated and the sequences of solutions generated were analyzed.

In order to utilize the level-set method, a continuous distribution of the level-set variable is required over the mesh. This is accomplished through an initialization step preceding the

primary simulation. In it, a velocity-independent version of Equation 3, shown in Equation 5, is utilized to solve for the scalar ϕ field. This differential equation is solved from $t_0 = 0$ to $t_f = 1$ μs using the PARDISO solver.

$$\frac{\partial \phi}{\partial t} = \gamma \nabla \cdot \left(\varepsilon_{ls} \nabla \phi - \phi(1-\phi) \frac{\nabla \phi}{|\nabla \phi|} \right) \quad (5)$$

After solving for a continuous level-set variable field, that field is provided to the second-stage solver. Equations 1-3 are solved simultaneously from $t_0 = 0$ to $t_0 = 8$ μs using the SPOOLES solver, with the output stored at steps of $\Delta t = 0.25$ μs. Each simulation utilized generalized-α time-stepping.

Generalized-α was found to be superior to the alternative BDF time-stepping algorithm because it was reliably able to take larger time steps and result in fewer solver failures due to divergence. The PARDISO and SPOOLES solvers are direct solvers (utilized because the relatively small number of degrees of freedoms) that were found to provide the most rapid results for their respective operation without a change in results.

After a series of preliminary simulations of the model to determine the proper order of magnitude of the actuation pressure, a series of simulations were run to determine the correlation between the droplet volume dispensed during a simulation and the gas reservoir pressure. Actuation pressure magnitudes ranging from 1.0 to 1.8 MPa were simulated.

For each simulation, there were two possible results, as illustrated in Figure 3. For actuation pressures 1.2 MPa or less, the droplet formed at the nozzle did not separate from the liquid reservoir, as shown in Figure 3(a) for a pressure magnitude of 1.0 MPa. For actuation pressures 1.3 MPa and greater, the droplet would form at the nozzle and retain sufficient velocity to overcome the fluid viscosity and surface tension, as shown in Figure 3(b) for a pressure magnitude of 1.4 MPa.

To enable quantitative comparison of the simulations, the gas pressure and droplet volume were calculated from the models. A point probe was placed in the gas reservoir to record the pressure in a data array over time. A surface integral was utilized to extrapolate the droplet volume. The integral was evaluated around the axis of symmetry, 20 μm below the nozzle, and when ϕ of the model exceeded 0.6.

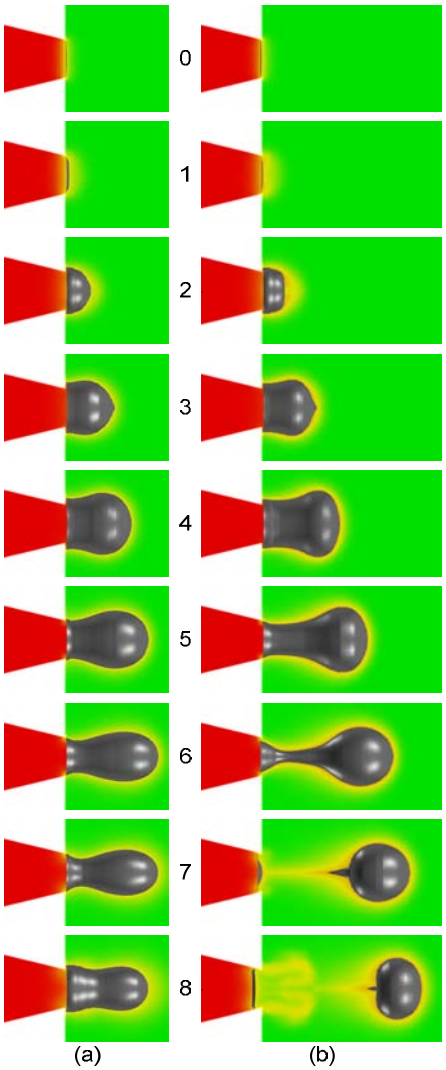

Figure 3. Droplet evolution: (a) without ejection, (b) with ejection (time in μs)

Figure 4 illustrates the time evolution of gas reservoir pressure during the simulation. It was determined that the best scalar metric for representing this function in the analysis was the maximum pressure measured in the gas reservoir. When these maximum pressures are plotted with the droplet volumes, an approximately linear relationship is found, as shown in Figure 5.

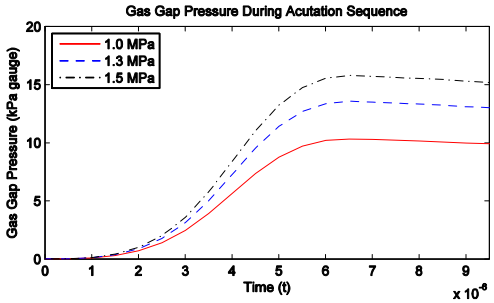

Figure 4. Pressure of the gas reservoir during simulation

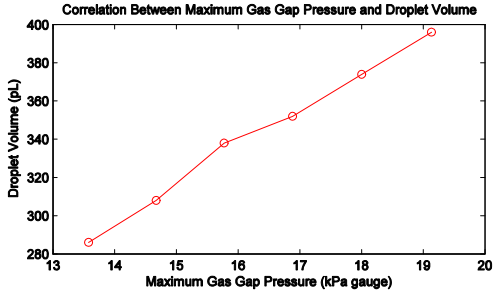

Figure 5. Correlation between gas reservoir pressure and ejected droplet volume

4. Conclusions

In this paper, an FE model was developed capable of demonstrating the feasibility of a novel sensing paradigm for measuring the volumes of dispensed microdroplets in real-time. A linear correlation between the droplet volume dispensed and the maximum pressure of a compressible gas reservoir was observed and quantified.

Future work will incorporate both more advanced simulations and experimental validation of this concept. The advanced simulations will be developed with COMSOL and utilize the fluid-structure interaction and piezoelectric physics modules to directly model the system under consideration. Preliminary experiments will also be conducted to empirically verify the findings.

5. References

1. M. Schena, R.A. Heller, T.P. Theriault, K. Konrad, E. Lachenmeier and R.W. Davis, Microarrays: biotechnology's discovery platform for functional genomics, *Trends Biotechnol.*, **16**, 301-306 (1998)

2. M. Zhang, O. Ma and X. Diao, Dynamics modeling and analysis of inkjet technology-based oligo DNA microarray spotting, *IEEE Trans. Autom. Sci. Eng.*, **3**, 159-168 (2006)

3. B. De Heij, B. Van Der Schoot, H. Bo, J. Hess and N.F. De Rooij, Characterization of a fL droplet generator for inhalation drug therapy, *Sens. Actuators A Phys.*, **85**, 430-434 (2000)

4. S. Yuan, Z. Zhou, G. Wang and C. Liu, MEMS-based piezoelectric array microjet, *Microelectron. Eng.*, **66**, 767-772 (2003)

5. G. Perçin, T.S. Lundgren and B.T. Khuri-Yakub, Controlled ink=jet printing and deposition of organic polymers and solid particles, *Appl. Phys. Lett.*, **73**, 2375-2377 (1998)

6. T.M. Lee, T.G. Kang, J.S. Yang, J.D. Jo, K.Y. Kim, B.O. Choi and D.S. Kim, 3D metal microstructure fabrication using a molten metal DoD inkjet system, *Int. Solid-State Sens. Actuators Microsyst. Conf.*, 1637-1640 (2007)

7. P. Ben-Tzvi and W. Rone, Microdroplet generation in gaseous and liquid environments, *Microsyst. Technol.*, **16**, 333-356 (2010)

8. J.R. Castrejón, G.D. Martin, S.D. Hoath and I.M. Hutchings, A simple large-scale droplet generator for studies of inkjet printing, *Rev. Sci. Instrum.*, **79**, 075108 (2005)

9. W.T. Berggren, M.S. Westphall and L.M. Smith, Single-pulse nanoelectrospray ionization, *Anal. Chem.*, **74**, 3443-3448 (2002)

10. T.N. Chang, S. Parthasarathy, T. Wang, K. Gandhi and P. Soteropoulos, Automated liquid dispensing pin for DNA microarray applications, *IEEE Trans. Autom. Sci. Eng.*, **3**, 187-191 (2006)

11. N. Szita, R. Sutter, J. Dual and R.A. Buser, A micropipettor with integrated sensors, *Sens. Actuators A Phys.*, **89**, 112-118 (2001)

12. P. Ben-Tzvi, R. Ben Mrad and A.A. Goldenberg, A conceptual design and FE analysis of a piezoceramic actuated dispensing system for microdrops generation in microarray applications, *Mechatron.*, **17**, 1-13 (2007)

13. P. Ben-Tzvi, *A dispensing system for microdrops generation in medical applications*, LAP Lambert Academic Publishing, Germany (2010)

14. H.C. Wu, H.J. Lin and W.S. Hwang, A numerical study of the effect of operating parameters on drop formation in a squeeze mode inkjet device, *Model. Simul. Mater. Sci. Eng.*, **13**, 17-34 (2005)